Desalination and Water Treatment
www.deswater.com
doi: 10.5004/dwt.2021.27915

244 (2021) 263–278
December

Fabrication of a novel chitosan Schiff bases hydrogel derivatives for the removal of anionic dyes from wastewater

R.E. Khalifa, S. Aboulhadeed, H.M. Ahmed, A.M. Omer, T.M. Tamer, M.S. Mohy-Eldin*

Polymer Materials Research Department, Advanced Technologies and New Materials Research Institute, City of Scientific Research and Technological Applications (SRTA-City), New Borg El-Arab City, P.O. Box: 21934 Alexandria, Egypt, Tel. +20 34593414; emails: mmohyeldin@srtacity.sci.eg (M.S. Mohy-Eldin), ORCID: 0000-0003-2228-211X, emails: randaghonim@gmail.com (R.E. Khalifa), s.a.aboulhadeed@gmail.com (S. Aboulhadeed), malak.scientist@gmail.com (H.M. Ahmed), amomar@srtacity.sci.eg (A.M. Omer), tmahmoud@srtacity.sci.eg (T.M. Tamer)

Received 24 May 2021; Accepted 25 October 2021

ABSTRACT

In this research, eco-friendly chitosan Schiff base hydrogel derivatives, as new adsorbents for anionic dye, Methyl orange (MO), were synthesized via coupling with 4-dimethylamino benzaldehyde (chitosan Schiff base (I)) and benzophenone (chitosan Schiff base (II)). The adsorbents' structure was examined and characterized by Fourier-transform infrared spectroscopy, scanning electron microscopy, thermogravimetric analysis, and differential scanning calorimetry. The MO adsorption percentage of the developed chitosan Schiff bases hydrogels compared to native chitosan was studied using a batch adsorption system under different adsorption conditions. The equilibrium time reached after 40 min for the chitosan Schiff bases adsorbents, while it was found 120 min for the chitosan adsorbent and the adsorption kinetics were found to follow the pseudo-second-order model. The values of α estimated by Elovich kinetic model are 2.2786 and 2.0489 mg/g which close from the experimental values; 2.415 mg/g for chitosan Schiff base (I), and chitosan Schiff base (II). Following up the adsorption mechanism performed using intraparticle diffusion model. The obtained results indicate the governed of the MO diffusion onto chitosan Schiff bases (I) and (II) by the boundary layer effect only. While that the removal process was governed by both surface removal and intraparticle diffusion in case of the chitosan adsorbent. At the same time, the Freundlich isotherm, Langmuir, and Temkin isotherm models have been applied to the adsorption data and were found to follow the Freundlich isotherm. The Langmuir monolayer maximum adsorption capacities were found 19.92, 19.34, and 22.37 mg/g for the chitosan, chitosan Schiff base (I), and chitosan Schiff base (II), respectively. The thermodynamic nature of the adsorption process was extracted using Van't Hoff plot. The positive values for the ΔH indicate the endothermic nature of the adsorption process.

Keywords: Hydrogel; Chitosan; Schiff bases; Methyl orange; Adsorption capacity; Kinetics; Isotherms; Thermodynamics

1. Introduction

The accelerated growth of world populations raises the need for regenerative water resources. The progress for many industries, especially the textile ones, depends mainly on consuming large amounts of water and coloured wastewater resulted at the end, which proposed the reuse of wastewater as a logical solution to respond to the continuous water demands. The resulted wastewater from textile industries mainly has low transparency and is coloured caused by very few amounts of dyes [1,2]. The anionic dyes contribute to the dying processes due to their ability

* Corresponding author.

to dye a wide range of materials [3–5]. Depending on the materials dying capability, from 10% to 50% of the anionic dyes are released in the wastewaters during the dyeing process [6]. The weak biodegradability of the anionic dyes comes mainly from their aromatic moieties and results in an induced serious hazards to aquatic living organisms [7,8]. Many dye removal techniques, including ion exchange, coagulation and flocculation, adsorption, advanced oxidation and extraction (AOP), membrane filtration and biological methods, have been investigated. However, most of these methods have their drawbacks, like the operational and capital costs, which are considered limiting factors in applying most of these methods. In addition, there are specific problems regarding sludge disposal and production of hazardous by-products. The biological methods are not regarded as effective and appropriate; time-consuming fermentation processes required for most of these methods and also inability to remove dyes consistently are the main disadvantages, while adsorption shows many advantages such as; simple design, ease and low operational cost, insensitivity towards the toxic compounds and removal efficiency even at low concentrations of contaminants, nominate it as first choice [9]. Chitosan, among other bio-sorbents, was investigated as an adsorbent for transition metal ions, organic species as well as coloured material studies [10–16]. Ho et al. [10] investigate the sorption of basic dye, Basic Red 13, from an aqueous solution using tree fern as biosorbent. Crini [11] reviewed non-conventional low-cost adsorbents for dye removal. Among them, activated carbon from solid agricultural wastes was extensively discussed. Fiorentina et al. [12] studied reactive blue 5G dye biosorption onto drying orange bagasse in a batch system.

Simple chemical transformation and modifications are induced due to the possession of different functional groups like amino (NH_2) and hydroxyl (OH) groups along the chitosan backbone [17–20]. Among these modifications, Schiff bases obtained by reaction of free amino groups of chitosan with active carbonyl compounds such as aldehyde or ketone are considered the most straightforward transformation [21,22]. Moreover, these Schiff bases' obtained (–RC=N–) groups offer several potential analytical and environmental applications by enhancing the adsorption/complexation properties [23,24].

Eco-friendly chitosan Schiff base hydrogel derivatives were synthesized in this research via coupling with 4-dimethylamino benzaldehyde and benzophenone. The hydrogels' structure was examined and characterized by Fourier-transform infrared spectroscopy (FTIR), scanning electron microscopy (SEM), thermogravimetric analysis (TGA), and differential scanning calorimetry (DSC). In addition, Methyl orange (MO) sorption properties of the developed chitosan Schiff bases hydrogels compared to native chitosan was studied via batch adsorption system under different operational conditions.

2. Materials and methods

2.1. Materials

Chitosan (molecular weight: 100,000–300,000 and degree of deacetylation ≥75%) was obtained from ACROS Organics (USA). Acetic acid (99.8%), hydrochloric acid (37%), Methyl orange (ACS reagent, dye content 85%), 4-dimethylamino benzaldehyde, and benzophenone were all purchased from Sigma-Aldrich (Germany). Sulfuric acid (98%), sodium hydroxide, and phenolphthalein were purchased from El-Nasr Pharmaceutical Co for Chemicals (Egypt).

2.2. Methods

2.2.1. Preparation of N-functionalized chitosan Schiff base

N-functionalized chitosan Schiff bases were prepared by modifying Soliman et al. method [25]. In detail, 1 g of the chitosan was dissolved in 50 mL acetic acid solution (2%) at ambient temperature overnight. First, filtration of chitosan solution was carried out using cheesecloth to remove un-dissolved chitosan. Then a 10 mL of absolute ethanol was added carefully to the chitosan solution, with continuous stirring to have a homogenous solution. Next, 31 mmol of 4-dimethylamino benzaldehyde or benzophenone previously dissolved in 10 mL ethanol were added to the above solution. After that, the temperature was rose to 70°C; the reaction mixture was left to react under continuous stirring for 6 h. Then 5 mL of 10% glutaraldehyde was added to the solution with continuous stirring at 70°C for an additional 1 h. The obtained gels were collected by filtration, washed several times with ethanol to remove any un-reacted aldehydes, and dried at 60°C under reduced pressure. Two different hydrogels were prepared using 4-dimethylamino benzaldehyde and benzophenone coded as Schiff base (I) and Schiff base (II). Both Schiff bases were characterized and evaluated comparing to chitosan hydrogel (Ch).

2.3. Characterization

2.3.1. Physicochemical characterization

2.3.1.1. Water uptake (%)

The water uptake (%) behaviour of the prepared hydrogel was investigated using distilled water. Accurately weighed amounts of hydrogels were immersed in water for 24 h at 37°C. The swollen hydrogel was periodically separated, and the adhered water to the surface of the hydrogel was removed by blotting them gently in between two filter papers, immediately followed by weighing. The water uptake (%) of the samples was determined according to the following formula [26]:

$$\text{Water uptake}\left(\%\right) = \left[\frac{\left(M_s - M_0\right)}{M_0}\right] \times 100 \quad (1)$$

where M_s is the weight of the swollen hydrogel and M_0 is the initial dry weight.

2.3.1.2. Ion-exchange capacity

A known weight of chitosan or Schiff base hydrogel was added to 20 mL of 0.1 M H_2SO_4 solution, and the mixture was kept under shaking for 3 h. Then, the mixture was filtered, and an aliquot was titrated against a standard sodium

hydroxide solution. Similarly, control titration without the addition of chitosan was also run. From the difference in the volume of 0.1 M NaOH required for neutralization, the ionic exchange capacity was calculated using the following equation:

$$\text{Ion exchange capacity} = \frac{\left(V_2 - V_1\right) A}{W\left(\text{meq/g}\right)} \quad (2)$$

where V_2 and V_1 are the volumes of NaOH required for complete neutralization of H_2SO_4 in the absence and presence of chitosan or chitosan Schiff bases hydrogel, respectively, A is the normality of NaOH and W is the weight of the sample taken for analysis [27].

2.3.1.3. Fourier-transform infrared spectroscopy

Infrared spectra were performed with Fourier transform infrared spectrophotometer (Shimadzu FTIR-8400 S, Japan) to confirm modification and prove the structure of the developed chitosan or chitosan Schiff bases hydrogel.

2.4. Thermogravimetric analysis

Analysis by TGA of samples was carried out using a thermogravimetric analyzer (Shimadzu TGA-50, Japan) under nitrogen, at a gas flow rate of 20 mL/min, to evidence changes in structure as a result of the modification. In addition, samples were measured their weight loss starting from room temperature to 600°C at a heating rate of 10°C/min.

2.5. Differential scanning calorimetry

Differential scanning calorimetric analysis of chitosan and chitosan Schiff base samples was carried out using differential scanning calorimeter device (Shimadzu DSC-60A, Japan) in the temperature range ambient to 350°C at a heating rate of 10°C/min under nitrogen flow (30 ml/min).

2.6. Scanning electron microscopy

Samples were coated under a vacuum with a thin layer of gold before being examined by scanning electron microscopy. Morphological changes of the sample's surface were followed using a secondary electron detector of SEM (Joel JSM 6360LA, Japan). Two magnifications factors were used; 1,000X and 5,000X under 10 KeV.

2.7. Batch equilibrium studies

The stock solution of MO dye (1,000 ppm) was prepared then the used concentrations were obtained by dilution. All the adsorption experiments were conducted in 100 mL flasks by adding a given amount of adsorbent to 25 mL dye solution of different dye concentrations with different pH values and shaking in an orbital shaker for a given time. The dye concentrations in the initial and final aqueous solutions were measured at 465 nm using UV-Vis spectrophotometer model 33C-B (Pharmacia Biotech. Co., Cambridge, England). The amount of dye adsorbed was calculated from the difference between the initial concentration and the equilibrium one. The values of percentage removal and the amount of dye adsorbed were calculated using the following relationships:

$$\text{Dye removal}\left(\%\right) = \frac{\left(C_0 - C_e\right)}{C_0} \times 100 \quad (3)$$

$$\text{Adsorption capacity}\left(\text{mg/g}\right) = \left[\frac{\left(C_0 - C_e\right)}{m}\right] \times V \quad (4)$$

where C_0 is the initial dye concentration and C_e is the final dye concentration in supernatant, m is the mass of the adsorbent (g), and V is the volume of the dye solution.

3. Results and discussions

In the current research, new chitosan Schiff bases hydrogel was prepared via coupling chitosan amine groups with 4-dimethylamino benzaldehyde or benzophenone followed by crosslinking with glutaraldehyde (Fig. 1). The prepared chitosan Schiff bases hydrogel was characterized using different characterization tools. The obtained chitosan Schiff bases hydrogel was evaluated as a dye removal material using Methyl orange as a model for anionic dye.

3.1. Characterization

3.1.1. Physicochemical characterization

Ion-exchange capacity confirms consumption of chitosan amine groups in coupling with aldehydes. Fig. 2 shows a decrease in chitosan hydrogel's ion-exchange capacity (4.45 meq/g) by reaction with 4-dimethylamino benzaldehyde, chitosan Schiff base hydrogel (I), and benzophenone, chitosan Schiff base hydrogel (II), to reach 3.19 and 2.19 meq/g, respectively. This result confirms the decrease of free amine content in the prepared chitosan Schiff bases. The result refers to a decrease in the ion exchangeability of aromatic amine derivatives in the substituted Schiff base (I) compared to aliphatic amine groups of chitosan. The water uptake shows a similar behaviour where decrease by Schiff base formation. These phenomena can be attributed to replacing hydrophilic amine groups of chitosan with hydrophobic aromatic groups. The water uptake (%) of chitosan Schiff base hydrogel (II) is much lower than the chitosan Schiff base hydrogel (I) due to the presence of two aromatic groups in the structure of the chitosan Schiff base hydrogel (II) compared with only one of the chitosan Schiff base hydrogel (I).

3.1.2. Infrared spectrophotometric

FTIR of chitosan and its Schiff bases hydrogel was performed and presented in Fig. 3. Charts demonstrate the functional characteristic bands of the polysaccharide of the chitosan backbone. Broadband at 3,200–3,600 cm^{-1} corresponds to the stretching vibration of OH and NH_2. The broadband Schiff base hydrogel intensity changes

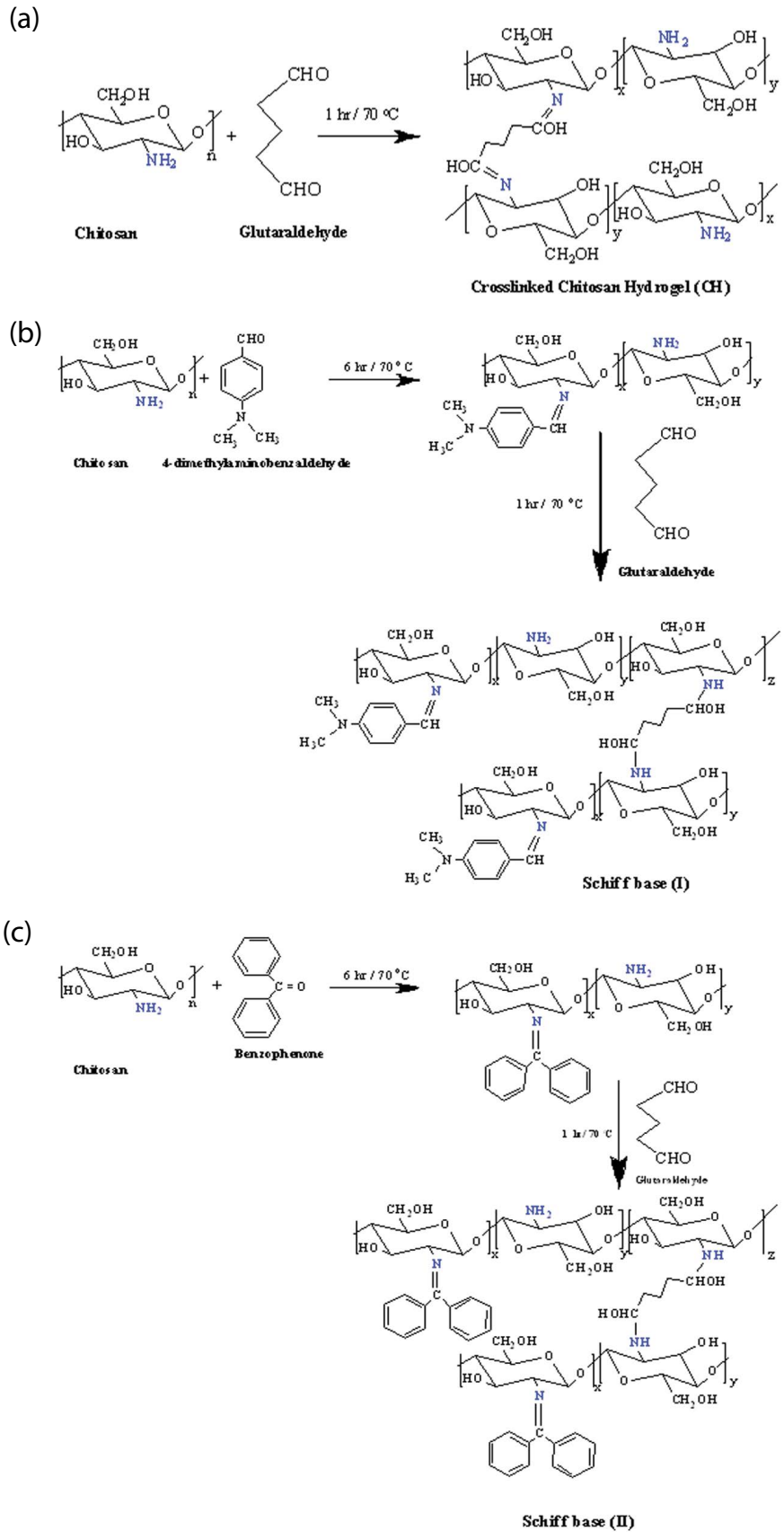

Fig. 1. Schematic preparation of: (a) chitosan, (b) chitosan Schiff base (I), and (c) chitosan Schiff base (II) adsorbents.

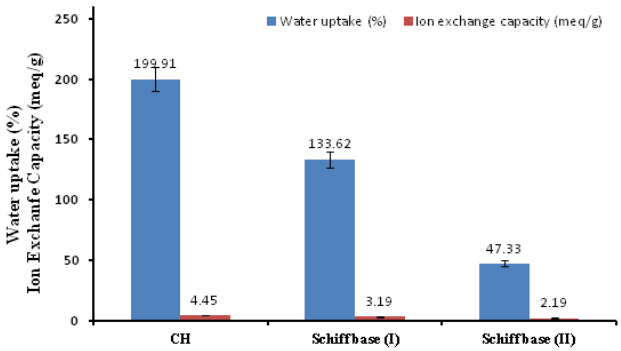

Fig. 2. Water uptake (%) and ion-exchange capacity of chitosan and chitosan Schiff bases adsorbents.

show that the amine groups (–NH_2) have been consumed in the Schiff base formation. Group of peaks at 2,850–1,960 cm^{-1} refer to the aliphatic C–H bond were recognized. The appearance of the new band at 3,048 and 3,054 cm^{-1} for chitosan Schiff base (I) and (II) respectively attributed to aromatic C–H vibration. The transmittance was reduced in the range of 1,000–1,300 cm^{-1}, related to C–O stretching vibrations of the chitosan chemical structure. Besides, the appearance of a small peak at 1,467 cm^{-1}, associated with secondary amine groups of the nitrogen atoms in the carbon C-2 groups of chitosan. Significant peaks observed in the Schiff base hydrogels in the range 1,400–1,600 cm^{-1} and 660 cm^{-1} were attributed to the aromatic rings of the immobilized groups.

3.1.3. Thermogravimetric analysis

The thermal stability of chitosan and its Schiff bases hydrogels was investigated using thermal gravimetric analysis. chitosan hydrogels exhibited three degradation behaviours in Fig. 4. The first weight loss around 100°C that attributed to the elevation of piping water content trapped using hydrophilic groups along the polymer backbone (i.e., –OH and –NH_2). Chitosan hydrogel demonstrates lower water content than its Schiff base hydrogels with values 11.41%, 12.52% and 16.09% for Ch, Schiff base (I) and (II) at 150°C, respectively. That can explain by the pseudo hydrophilic nature of porous surfaces [28]. The second weight loss was recognized at 220°C–320°C. That refers to distractive degradation of the chitosan glucose ring [29]. The loss of 50% of the tested samples at 385.88°C, 409°C and 314.45°C for Ch, Schiff base (I) and (II), respectively, indicates the immobilized Schiff base on the thermal stability of the developed adsorbents. The third degradation stage at a higher temperature has resulted in the degradation of the formed residue in the previous step [29].

3.1.4. Differential scanning calorimetry

Fig. 5 exhibits the DSC curves of chitosan and its Schiff bases hydrogels. The endothermic peaks before 100°C refer to an elevation of in piping moisture content attached to the polymer, where recognized at 90°C, 80°C, and 65°C for the chitosan, chitosan Schiff base (I),

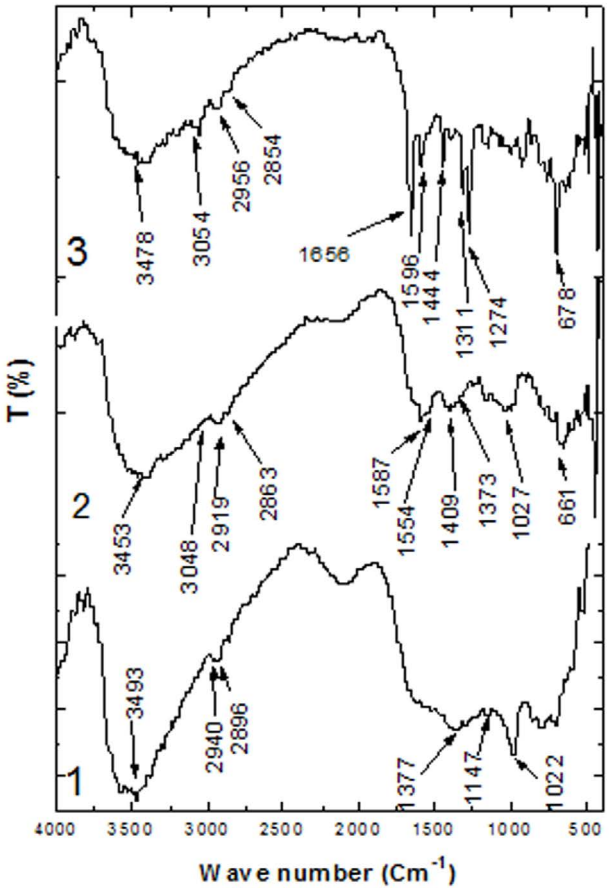

Fig. 3. FTIR of: (1) chitosan, (2) chitosan Schiff base (I), and (3) chitosan Schiff base (II) adsorbents.

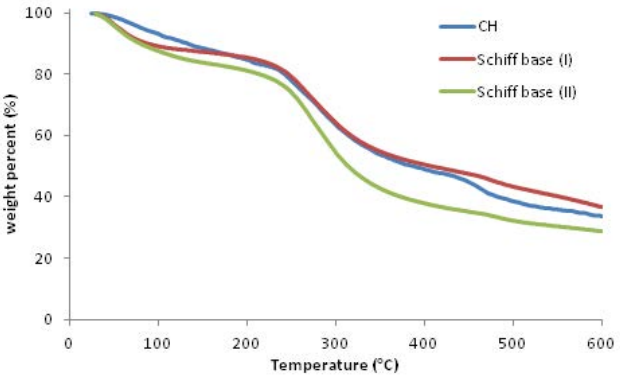

Fig. 4. TGA of chitosan (Ch), chitosan Schiff base (I) and chitosan Schiff base (II) adsorbents.

and chitosan Schiff base (II), respectively. The noticed shift is strongly related to the hydrophilicity of the matrices where the chitosan has 200% water uptake, while chitosan Schiff base (I), and chitosan Schiff base (II), have 134% and 47%, respectively. The first exothermic peaks, which appear in the temperature range at about 250°C, correspond to the thermal degradation of the polysaccharide pyranose

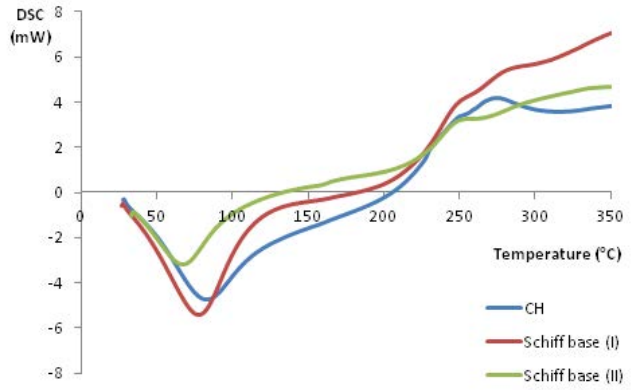

Fig. 5. DSC of chitosan (Ch), chitosan Schiff base (I) and chitosan Schiff base (II) adsorbents.

ring. The observed behaviour follows our previously published results [28]. The second exothermic peaks which appear in the temperature range at about 250°C–300°C; chitosan at about 275°C, while chitosan Schiff base (I), and chitosan Schiff base (II) appear at 285°C and 300°C, respectively, may be related to the decomposition of amine units [30]. The shift and broadening of this peak in case of the Schiff base (I) and (II) as attributed to more minor amine groups due to the formation of Schiff bases from one side and the hydrophobicity of the immobilized aromatic ring with two terminal methyl groups of the Schiff base (I), and the immobilized two aromatic rings of the Schiff base (II). Similar behaviour was observed by other authors [31] and through our previously published work [32].

Dos Santos et al. [33] studied the thermal behaviour of six biopolymeric Schiff bases obtained from the reaction of chitosan and salicylaldehyde derivatives. They observed a broad endothermic peak in the DSC curves of chitosan around 83°C related to the loss of water, whereas the exothermic peak at 303°C corresponds to the decomposition of the biopolymer. The Schiff bases presented similar DSC profiles, but the endothermic peaks were shifted to lower temperatures than the chitosan itself. Meanwhile, the exothermic peaks were shifted to higher temperatures compared to the pure chitosan.

3.1.5. Scanning electron microscopy

The morphological analysis of chitosan and its Schiff base derivatives presented in Fig. 6 show transformation of the chitosan Schiff bases morphology where turned to porous structure with coupling chitosan with 4-dimethylamino benzaldehyde, Schiff base (I), and benzophenone; Schiff base (II). The Schiff base (II) has a higher porosity than the Schiff base (I); magnification 5,000X. That can be explained by the presence of side chains with a terminal methylated aromatic ring in the case of the Schiff base (I) and side-chains with a terminal two aromatic rings in the case of the Schiff base (II) hydrogels. These chains increase the spacing between polymer chains. In addition, replacing hydrophilic amine groups with hydrophobic aromatic groups can distort the polymer crystal structure [34].

3.2. Adsorption process

In this work, we investigated the sorption behaviour of MO from contaminated water by chitosan and its Schiff bases hydrogels. Batch experiments were performed. The adsorption behaviours of the hydrogels towards the MO were studied under different operational conditions; MO concentration, adsorption time, adsorption temperature, adsorption pH, agitation rate and adsorbent dosage.

3.3. Effect of the adsorption' time and sorption kinetics

Fig. 7 illustrates the adsorption process as a function in time. The ability to MO removal was increased as the contact time increase. It is recognized that MO removal has almost been completed after only 15 min, where 87% and 93% removal percentage for Schiff bases (I) and (II) were reached. Then the slight increase of the removal percentages to about 95% was obtained after further 25 min, where the equilibrium was reached at 40 min adsorption time for Schiff bases (I) and (II). A slower rate of adsorption behaviour was observed by chitosan, where only 33% of MO was removed after 15 min, and the equilibrium was reached after 120 min, where about 85% of MO was removed. However, the experiment was conducted for 180 min to make sure that a complete equilibrium was attained.

This phenomenon was attributed to the fact that many active surface sites were available for adsorption at the initial stage, in addition to different charges between adsorbent surface and dye molecules. Then competition between dye molecules to the remaining vacant surface sites with the same charge of previously adsorbed dye molecules challenged the adsorption process closed to equilibrium.

The ion-exchange capacity of the prepared chitosan Schiff bases had shown a decrease in the absorbent charge compares to chitosan. Many studies linked positive chitosan charges and their affinity to anionic dye [35–37]. Contrarily, the chart demonstrates the promotion of adsorption capacity by consuming amine groups and S chitosan Schiff bases formation. The performance of chitosan involves two factors, mainly hydrophobic interactions and the possibility of chain association through hydrogen bridges. The hydrophobic interactions are due to the methyl group of the acetamide function (in partial acetyl amine groups) and to the –CH and $–CH_2$ groups of the glucose ring.

Immobilization of aldehyde molecules on chitosan let increase the hydrophobic interaction between dye and chitosan surface. Moreover, crystal structure distortion generates a rough and porous microstructure that produces a higher adsorbent surface area.

For a better understanding of the sorption process, the obtained data were treated by various kinetic models, namely; pseudo-first-order and pseudo-second-order models, to recognize the possible rate-controlling steps involved in the process of adsorption [38,39]; Fig. 7b–c. The kinetic models are represented by the following linear form Eqs. (5) and (6);

$$\ln\left(q_e - q_t\right) = \ln q_e - k_1 t \tag{5}$$

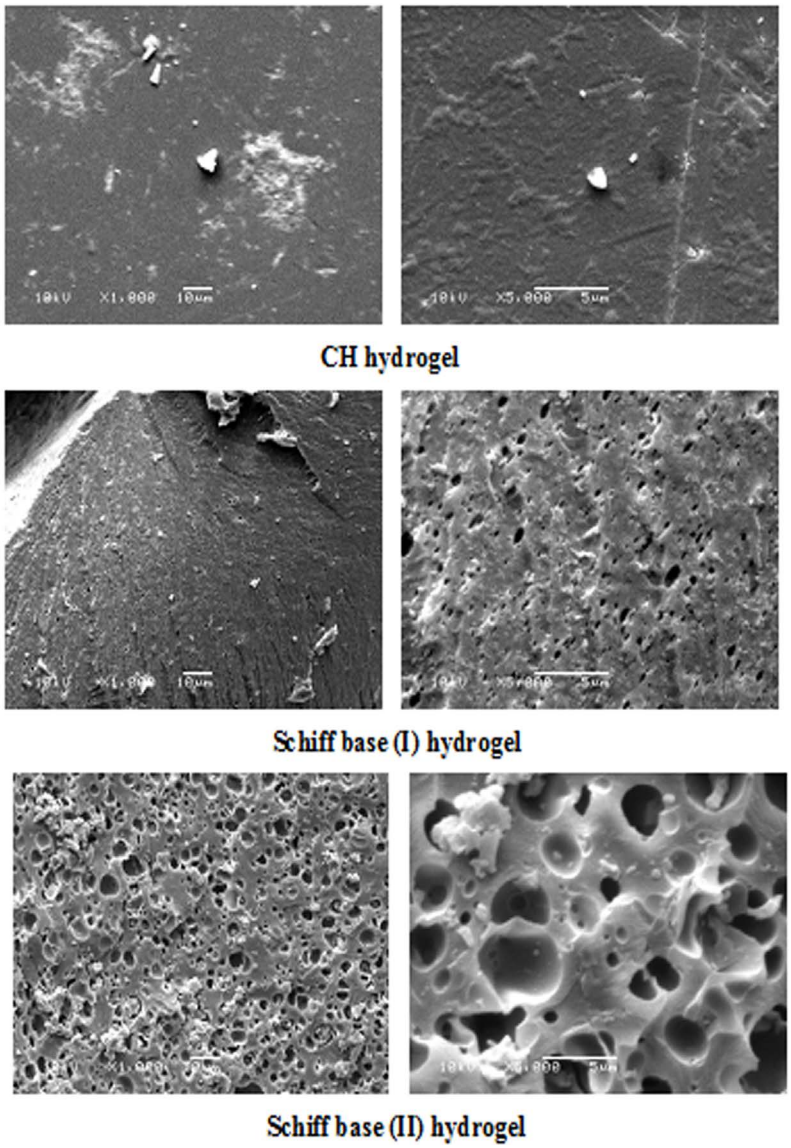

Fig. 6. SEM pictures of chitosan (Ch), Schiff base (I) and Schiff base (II) hydrogels.

$$\frac{t}{q_t} = \frac{1}{k_2 q_e^2} + \frac{t}{q_e} \tag{6}$$

where q_e and q_t (mg/g) are the MO dye sorption capacity at equilibrium and time t (min). k_1 (min^{-1}) and k_2 (g/g min) are the pseudo-first-order and pseudo-second-order sorption's constant rate parameters. The kinetic parameters extracted from Fig. 7b–c are tabulated in Tables 1 and 2.

From the tabulated results, it is evident that the sorption process data fitted very well with the pseudo-second-order models since they provided fair values of the correlation coefficient (all values of R^2 are close to 1). The theoretical (q_{exp}) and the figured (q_{cal}) values of the MO adsorption capacity are presented in Tables 1 and 2 and indicated that the sorption behaviour of chitosan Schiff bases adsorbents is best described by the pseudo-second-order models [40]. This result agrees with many published results [41,42–45], which demonstrated that the kinetic of MO adsorption process fitted well with pseudo-second-order reaction kinetic.

The simple Elovich model recently has also been applied to describe the adsorption process kinetic of pollutants from aqueous solutions using linear form of the following equation [46]:

$$q_t = \alpha + \beta \ln t \tag{7}$$

The Elovich constants are α (mg/g min), the initial sorption rate, and β (g/mg); the extent of surface coverage and activation energy for chemisorption.

Fig. 7d illustrates the plot of q_t against ln$t$ for the sorption of the MO anions onto the chitosan and its Schiff bases (I) and (II). The estimated Elovich equation parameters were obtained (Table 3). The value of β is indicative of the number of sites available for adsorption, 0.5731, 0.0318,

Table 1
Adsorption parameters of pseudo-first-order kinetic model

Parameter	Ch	Schiff base (I)	Schiff base (II)
k_1 (min^{-1})	–0.0399	–0.0189	–0.0244
$q_{e,cal}$ (mg/g)	3.1124	12.87	7.14
$q_{e,exp}$ (mg/g)	2.161	2.437	2.437
R^2	0.9814	0.9389	0.8332

Table 2
Adsorption parameters of pseudo-second-order kinetic model

Parameter	Ch	Schiff base (I)	Schiff base (II)
k_2 (min^{-1})	10.739	0.275	0.4832
$q_{e,cal}$ (mg/g)	2.56	2.44	2.45
$q_{e,exp}$ (mg/g)	2.161	2.437	2.437
R^2	0.9928	1.0	1.0

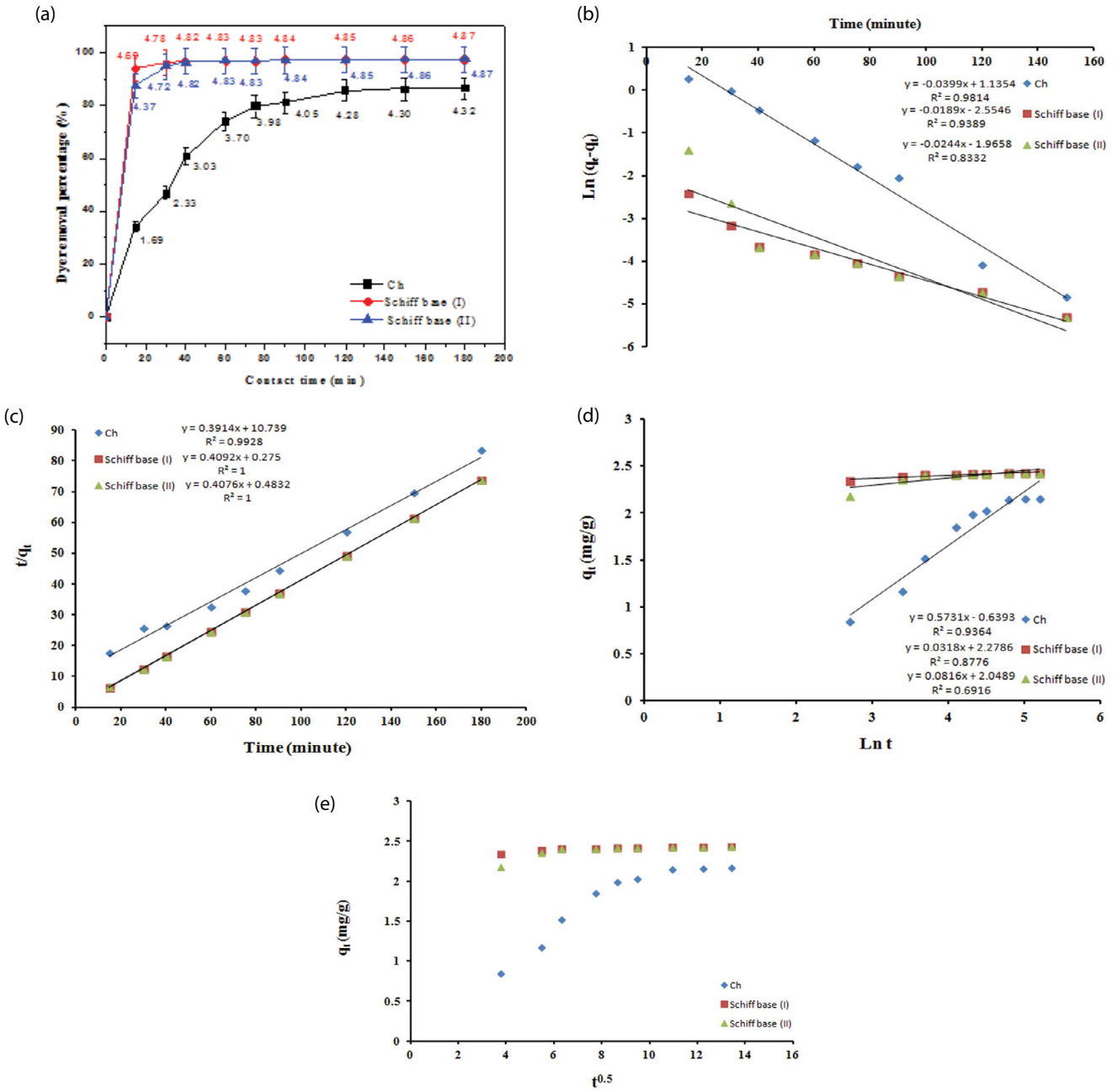

Fig. 7. (a) Effect of the adsorption' time on the removing percent (%) of MO using chitosan (Ch), chitosan Schiff base (I) and chitosan Schiff base (II) adsorbents (5 ppm MO, pH 4.0, 40°C, 250 rpm, 0.05 g), (b) pseudo-first-order model, (c) pseudo-second-order model, (d) Elovich model, and (e) intraparticle diffusion model.

Table 3
Adsorption parameters of Elovich kinetic model

Parameters	Ch	Schiff base (I)	Schiff base (II)
B (g/mg)	0.5731	0.0318	0.0816
α (mg/g min)	0.6393	2.2786	2.0489
R^2	0.9364	0.8776	0.6916

and 0.0816 g/mg for chitosan and chitosan Schiff bases (I) and (II), respectively. While α value is 0.6393, 2.2786, and 2.0489 mg/g, for chitosan and chitosan Schiff bases (I) and (II), respectively, is the adsorption quantity when ln$t$ is equal to zero, that is, the adsorption quantity when t is 1 h. The values of α, 2.2786 and 2.0489 mg/g, are close from the experimental values; 2.415 mg/g. These values are helpful in understanding the adsorption behavior of the first step [47].

Following up the adsorption mechanism of any ions onto solid from aqueous phase is going through a multi-step process. Initially, two steps are recognized in the liquid phase. The first step is the transport of the ions from the aqueous phase to the surface of the solid particles which is known as bulk diffusion. This step followed by diffusion of the ions via the boundary layer to the surface of the solid particles (film diffusion). The last step is, consequently, happened in the solid phase where the ions transport from the solid particles surfaces to its interior pores, known as pore diffusion or intraparticle diffusion. This step is likely to be slow and therefore, it may be considered as the rate-determining step.

The diffusion rate equations inside particulate of intra-particle model was used to calculate the diffusion rate of the MO anions onto the chitosan and chitosan Schiff bases (I) and (II). The adsorption process via intra-particle diffusion resistance [48] using the intra-particle diffusion model described as follows:

$$q_t = k_d t^{1/2} + I \tag{8}$$

The k_d is the intra-particle diffusion rate constant. Kannan et al [48] have figured out the thickness of the boundary layer from the values of I. Greater boundary layer effect was noticed with larger intercept [49]. The plot of q_t vs. $t^{0.5}$ was presented in Fig. 7e. Usually two separate linear portions that represent each line observed. These two linear portions in the intraparticle model suggest that the removal process consists of both surface removal and intraparticle diffusion. While the initial linear portion of the plot is the indicator of exist of the boundary layer effect, the second linear portion is due to intraparticle diffusion [50]. In our case, only one linear portion is obtained with very good R^2 values (0.989) chitosan Schiff bases (I) and (II) which indicates the exits of the boundary layer effect. Two separate linear portions that represent each line observed in chitosan curve suggest that the removal process consists of both surface removal and intraparticle diffusion. The intraparticle diffusion rate (k_d), 0.03315, 0.0033, and 0.0033 mg/g min, calculated from the slope and the values of I (the intercept); 1.7583, 2.3926, and 2.3926 mg/g provides an idea about the thickness of the boundary layer. The larger the intercept, the greater is the boundary layer effect [49]. Accordingly, the boundary layer effect in our case is higher in case of chitosan Schiff bases (I) and (II) adsorbents.

In case of involving the intraparticle diffusion in the sorption process, then a linear relationship would result from the plot of q_t vs. $t^{1/2}$, and the intraparticle diffusion would be the controlling step if this line passed through the origin [51]. Fig. 7e confirms straight lines not passed through the origin.

3.4. Effect of the adsorption' temperature

The effect of adsorption temperature, in the range between 25°C and 80°C, on the removal percent (%) of MO using chitosan and its Schiff bases adsorbents was investigated and the results presented in Fig. 8a. For chitosan adsorbent, the elevation of temperature shows improvement in the adsorption process. The increase of temperature enhances the mobility of the large dye ions and accelerates their random movements in solution; thus, it enhances the rate of collisions with the absorbent surface. Also, it produces a swelling effect on the internal structure of the absorbent, thus allowing the giant dye molecules to penetrate further. Therefore, the adsorption capacity largely depends on the interaction between the functional groups on the adsorbent surface and the adsorbate and should increase as the temperature rises [52]. There is no significant temperature effect on the prepared Schiff base adsorbents that can be referred to the high number of active adsorption sites compared to the available number of dye molecules for the tested sample.

From engineering aspects, the values of thermodynamic parameters such as the enthalpy change (ΔH), the free energy change (ΔG), and the entropy change (ΔS) should be taken into consideration to conclude the spontaneity of the adsorption process. An automatic system will display a decrease in ΔG and ΔH values with increasing the temperature. All the thermodynamic parameters calculated from the following equations [53,54]:

$$\ln K_d = \frac{\Delta S}{R} - \frac{\Delta H}{RT} \tag{9}$$

Where:

$$K_d = \frac{q_e}{C_e} \tag{10}$$

$$\Delta G = -RT \ln K_d \tag{11}$$

where R is the gas constant (8.314 J/mol K), and T is the temperature in K. Table 4 lists down the values for the thermodynamic parameters (Fig. 8b). The positive values for the ΔH indicate the endothermic nature of the process, which explains the increase of the MO anions adsorption efficiency as the temperature increased in the case of the chitosan adsorbent. A less significant effect of the temperature increase was noticed in the cases of the chitosan Schiff bases adsorbents. As informed by Alkan et al. [55], the enthalpy

Table 4
Thermodynamic parameters of the adsorption capacity for the MO dye by various chitosan adsorbents

Temperature (°C)	ΔG (kJ/mol)		
	Adsorbent		
	Ch	Schiff base (I)	Schiff base (II)
25	–0.0215	–0.077	–0.073
30	–0.0263	–0.076	–0.073
40	–0.0300	–0.077	–0.073
50	–0.0358	–0.074	–0.074
60	–0.0366	–0.072	–0.072
70	–0.0364	–0.070	–0.070
80	–0.0398	–0.068	–0.068
Adsorbent	Ch	Schiff base (I)	Schiff base (II)
ΔH (kJ/mol)	13.75	2.099	4.71
ΔS (J/mol K)	53.17	30.23	37.7

change values resulting from the chemisorption are between 40 and 120 kJ mol^{-1}, which are more significant than that caused by the physisorption. Consequently, the low values of the heat of adsorption acquired in this study indicate that the adsorption of the MO anions is probably attributable to the physisorption.

Conversely, in the kinetics study, it was described that the adsorption is chemisorption. Thus, it is evident from the low ΔH values that the physisorption also takes part in the adsorption process in which the MO anions adhere to the adsorbent active sites only through hydrophobic–hydrophobic interactions. The positive values for the entropy change, ΔS (53.17, 30.23, and 37.7 J/mol K), illustrating the disorderliness at the solid/liquid interface during the adsorption of the MO anions onto the chitosan and the chitosan Schiff bases adsorbents. The ΔG values reflect the feasibility of the process.

3.5. Effect of the agitation' rate

Fig. 9 shows the effect of varying the agitating rate from 50 to 250 rpm on adsorption of MO using chitosan and its Schiff base (I) and (II) hydrogels with constant kinetic parameters. The study shows two stages. The first stage, from 50 to 150 rpm, shows a significant increment of the MO adsorption percent (%), where doubled for Ch adsorbent and its Schiff base (I), while shows more significant improvement reaching 2.7 folds in the case of Schiff base (I). The second stage, from 150 to 250 rpm, shows a slower rate of MO removal (%) where the MO removal (%) improved by only 15%, 8% and finally 2% for the Ch adsorbent, the Schiff base (I) adsorbent, of the Schiff base (II) adsorbent, respectively, relative to their values at 150 rpm. These results can be associated with the fact that the agitation speed increases the diffusion of MO towards the surface of the adsorbents. Ruthven proposes that intraparticle diffusivity value hugely depends on adsorbents' adsorption capacity and surface properties (Ruthven, 1985) [56]. Thus, increasing the agitation rate will overcome the thickness of the liquid film and the mass-transfer resistance for the three tested adsorbent surfaces. Consequently, these also mean that a shaking rate of 150 rpm is sufficient to ensure that all the surface binding sites are made readily available for Methyl orange uptake for the chitosan Schiff base adsorbents [57,58].

3.6. Effect of the solution' pH

The adsorption process of MO by chitosan and its Schiff bases was examined in response to the solution' pH variations where the chitosan Schiff bases adsorbents show higher dye removal percent; Fig. 10a. As shown in the figure, a linear decrease in the dye removal ability of chitosan was observed when the solution' pH was varied from acidic to alkaline. That may be attributed to the ionization behaviour of amino groups of the chitosan chain. Chitosan has primary amino groups with a pKa value around 6.5 [59]. At pH below pKa of chitosan, the amino groups are

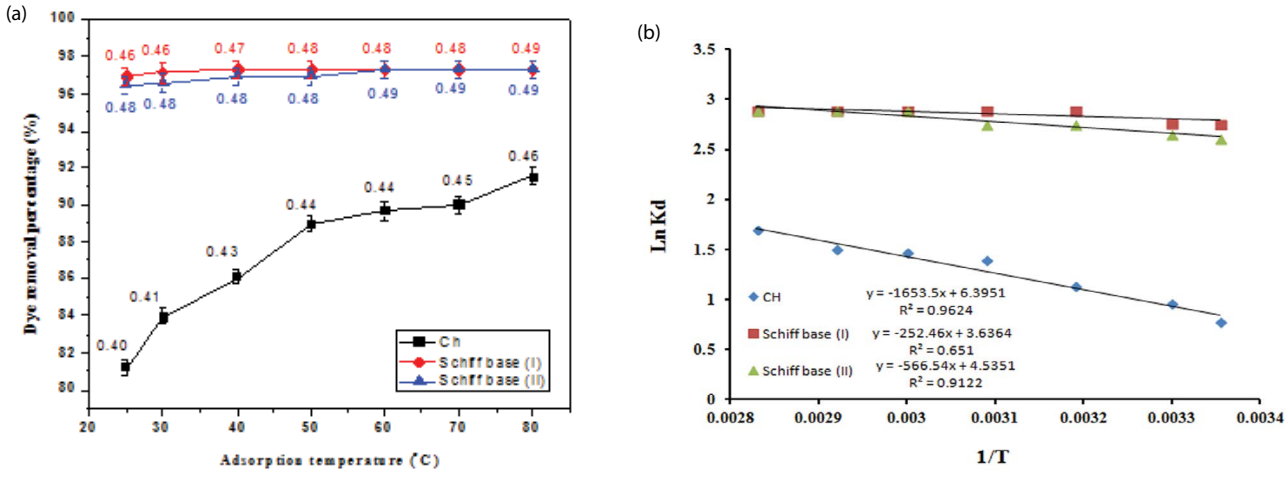

Fig. 8. (a) Effect of the adsorption' temperature on the removing percent (%) of MO using chitosan (Ch), chitosan Schiff base (I) and chitosan Schiff base (II) adsorbents (5 ppm MO, pH 4.0, 180 min, 250 rpm, 0.05 g) and (b) thermodynamics Van't Hoff model.

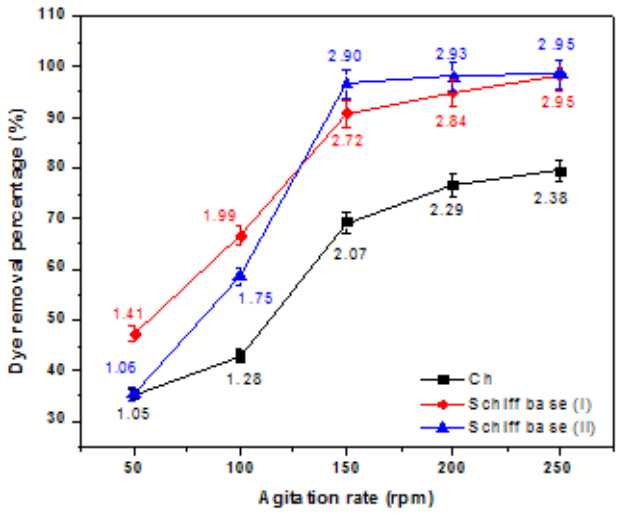

Fig. 9. Effect of agitation rate on the removing percent (%) of MO using chitosan (Ch), chitosan Schiff base (I) and chitosan Schiff base (II) adsorbents (5 ppm MO, pH 4.0, 180 min, 25°C, 0.05 g).

protonated and pair positively charged. Decreasing the pH of the dye solution offers more protons available to protonate the amine group of chitosan with the formation of a large number of cationic amines, which increases dye adsorption due to increased electrostatic interactions. At pH above the pKa, chitosan' amino groups are kept in the form of NH_2; the adsorption process was controlled only with hydrophobic interaction, leading to lower dye adsorption capacities. A certain amount of dye adsorption at higher pH implied the presence of different interactions in the adsorption process simultaneously, such as dye-dye interaction, dye-adsorbent, physical adsorption, and aggregation [60].

On the other hand, the chitosan Schiff bases show almost plateau dye removal percent (%) ranged between 90% and 95% at pH ranged between 4.0 and 9.0, which shows the dominant hydrophobic interactions role of the Schiff bases immobilized aromatic hydrophobic moieties in the adsorption process. At pH 10.0, the chitosan part in the chitosan Schiff bases lost the adherent water molecules and "precipitate", leading to reduce the pores nature of the chitosan Schiff bases and consequently the availability of the adsorbent active side to the MO molecules where chitosan Schiff base (I)' dye removal percent decreased from 90% at pH 9.0% to 74.4% at pH 10.0. While a sharp decline of the chitosan Schiff base (II)' dye removal percent from 92.54% at pH 9.0 to 47.79% at pH 10.0 was observed, showing the impact of higher hydrophobicity of the chitosan Schiff base (II), which was confirmed by the water uptake (%) results presented in Fig. 2.

To estimate the contribution of the Schiff bases formation in the dye removal percent, theoretical estimation of the amine group contents in both Schiff bases was performed based on the correlation between the IEC values of the chitosan, chitosan Schiff base (I) and chitosan Schiff base (II); 4.45 meq/g, 3.19 and 2.19 meq/g, respectively. Accordingly, the dye removal percent (%) values under different pH of the chitosan adsorbent was considered as reference (100%), and the dye removal percent (%) values of the chitosan Schiff base (I) and chitosan Schiff base (II) were 71.68% and 49%. The calculated theoretical dye removal percent (%) for the chitosan Schiff bases, dye removal percent (*T*) (%), were compared with the obtained experimental values for chitosan Schiff bases, dye removal percent (*E*) (%); Fig. 10a, and presented in Fig. 10b. The figure shows the difference between the expected dye removal percents for the chitosan Schiff bases due to the amine groups contents and their experimental counterparts where the hydrophobic–hydrophobic interaction occurs. The estimation of the synergetic impact of the hydrophobic–hydrophobic theoretical added values on the dye removal percents (%) for the chitosan Schiff bases is presented in Table 5. The table shows the increase of the synergetic effect with an increase of the adsorption' pH values for the chitosan Schiff bases. The obtained behaviour may be explained by changing the

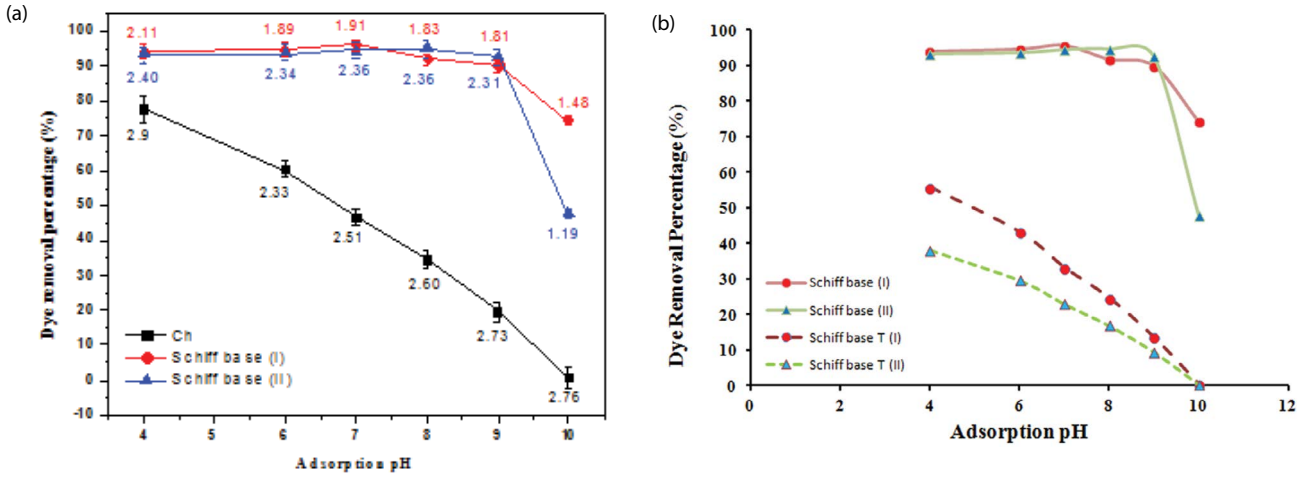

Fig. 10. (a) Effect of the adsorption' pH on the removing percent (%) of MO using chitosan (Ch), chitosan Schiff base (I) and chitosan Schiff base (II) adsorbents (5 ppm MO, 180 min, 25°C, 250 rpm, 0.05 g) and (b) theoretical MO removal percent of the chitosan Schiff base (I) and chitosan Schiff base (II) adsorbents.

Table 5
Theoretical dye removal percent (*T*), based on the amine groups content (degree of acetylating), of the chitosan Schiff bases compared with the experimental dye removal percent (*E*), and the estimated hydrophobic–hydrophobic added synergetic dye removal percent

pH	Dye removal percent (*E*) (%) Schiff base (I)	Dye removal percent (*T*) (%) Schiff base (I)	Hydrophobic–hydrophobic theo. added synergetic dye removal percent (%) Schiff base (I)	Dye removal percent (*E*) (%) Schiff base (II)	Dye removal percent (*T*) (%) Schiff base (II)	Hydrophobic–hydrophobic theo. added synergetic dye removal percent (%) Schiff base (II)
4	94.07	55.77	38.30	93.39	38.12	55.27
6	94.75	43.24	51.51	93.73	29.57	64.16
7	95.76	33.22	62.54	94.58	22.92	71.66
8	91.86	24.66	67.20	94.75	16.86	77.89
9	90.00	13.62	76.38	92.54	09.47	83.07
10	74.41	00.49	93.92	47.80	00.33	47.47

pHzpc values of the chitosan and the chitosan Schiff bases. The pHzpc of a solid is the pH at which the charge on the surface of the solid is neutralized; it becomes zero [61]. Thus, the surface of the solid is positively charged below pHzpc and negatively charged above pHzpc.

Jóźwiak et al. [62] studied the sorption capacity of chitosan having different deacetylation degrees (DD), namely, 75%, 85% and 90% relative to the Reactive Black 5 in a wide pH range – from 3 to 11. The sorption capacity was 433.03, 464.52, and 532.14 mg/g, respectively. They correlate the obtained results to the impact of the deacetylation degree on the sorbent's pHzpc (zero point of charge). Along with the increase in the deacetylation degree, the value of chitosan pHzpc increased as well and at DD = 75% DD = 85% and DD = 90%, pHzpc amounted respectively 7.6, 7.7 and 7.8.

The chitosan used in this study has DD = 75% and pHzpc value 7.6. Based on the IEC values, we can assume that the chitosan Schiff base (I) has DD = 52% and the chitosan Schiff base (II) has DD = 35%. According to the conclusion of Jóźwiak et al [56], the pHzpc values of the chitosan and the chitosan Schiff base (I) and (II) will following the order: chitosan > chitosan Schiff base (I) > chitosan Schiff base (II). That results in an additional contribution of the hydrophobic–hydrophobic interaction.

3.7. Effect of the adsorbent dose

The effect of the adsorbent dose on the MO removing percent (%) was examined by varying the adsorbent amount from 0.025 to 0.2 g using 20 mL of MO dye solution. The observed trend due to variation in chitosan and its Schiff bases (I) and (II) is represented in Fig. 11. It was observed that an increase in the adsorbent dose leads to an improvement in the absorption rate. That could be associated with the increasing adsorbent amount providing greater surface area and sorption sites [63,64]. Furthermore, it was remarked that after specific addition of dose, the removing percent of MO remains constant with further increase in adsorbent dose, which implied that the MO concentration gradient between the liquid phase (MO solution) and the solid phase (adsorbent) almost disappeared and consequently the driving force to move the MO molecules towards the adsorbent surface lost.

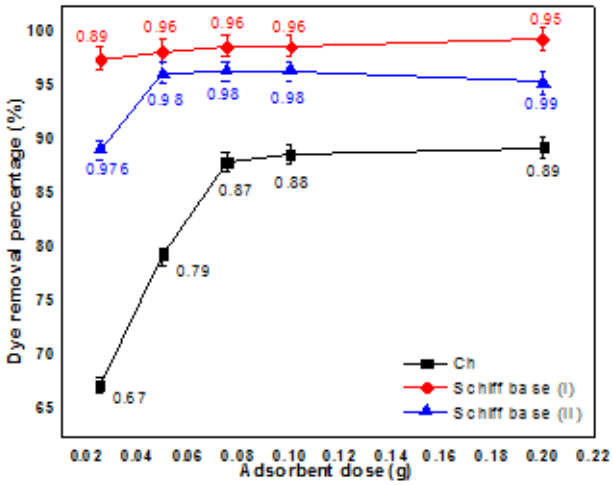

Fig. 11. Effect of adsorbent dose on the removing percent (%) of MO using chitosan (Ch), chitosan Schiff base (I) and chitosan Schiff base (II) adsorbents (5 ppm MO, pH 4.0, 180 min, 25°C, 250 rpm).

3.8. Effect of the MO concentration

Fig. 12a shows the effect of initial MO concentration on the removal percent (%). The removal percentage linearly reduced with an increase in initial MO concentration. This trend is due to the electrostatic repulsion between the dye molecules with increasing concentration, resulting in a competition between the dye molecules for the limited active sites in the adsorbent. A similar effect was observed with the other anionic dyes [3,19,64,65]. The obtained results follow the previously published result by the authors using chitosan derivate Schiff bases obtained from the coupling of chitosan with 1-vinyl 2-pyrrolidone and 4-amino acetanilide [66].

The results obtained on the adsorption of the MO anions onto the chitosan adsorbent and the chitosan Schiff bases were analyzed by the well-known models given by Freundlich and Langmuir using the linear forms of these kinds of isotherms.

The Freundlich model is the earliest known empirical equation and is consistent with an exponential distribution of active centres, characteristic of heterogeneous surfaces [67].

$$\ln q_e = \ln K_F + \frac{1}{n_f} \ln C_e \tag{12}$$

where K_F is the Freundlich constant depicts adsorption capacity, and n_f is a constant indicating adsorption intensity.

Linear fits of sorption data of the MO anions are given in Fig. 12b. According to the correlation coefficient (R^2) values 0.993, 0.9979, and 0.9944 for the chitosan adsorbent and the chitosan Schiff bases (I) and (II), respectively, it was demonstrated that the removal of the MO anions using the chitosan adsorbent and the chitosan Schiff bases (I) and (II) obeyed the Freundlich isotherm. The values of Freundlich constants n_f and K_F estimated from the slope and intercept of the linear plot were presented in Table 6. From the estimated value of n_f, it was found that $n_f > 1$ indicating favourable adsorption for the MO anions using the chitosan adsorbent and the chitosan Schiff bases (I) and (II) [68].

The Langmuir model, which is valid for monolayer sorption onto a completely homogeneous surface with a finite number of identical sites and with little interaction between adsorbed molecules, is given by the following equation [69]:

$$\frac{C_e}{q_e} = \frac{1}{q_m K} + \frac{C_e}{q_m} \tag{13}$$

where q_e is the amount adsorbed (mg/g), C_e is the equilibrium concentration of the adsorbate ions (mg/L), and q_m and K are Langmuir constants related to maximum adsorption capacity (monolayer capacity) (mg/g) and energy of adsorption (L/mg).

Fig. 12c illustrates the linear plot of the Langmuir equation for the MO anions removal using the chitosan adsorbent and the chitosan Schiff bases (I) and (II) at various initial MO anions concentrations ranged between 5 ppm and 50 ppm. The correlation coefficient (R^2) values are considered an indicator of the goodness-of-fit of experimental data on the isotherm's model. The R^2 values were 0.9793, 0.9553, and 0.9739 for the chitosan adsorbent and the chitosan Schiff

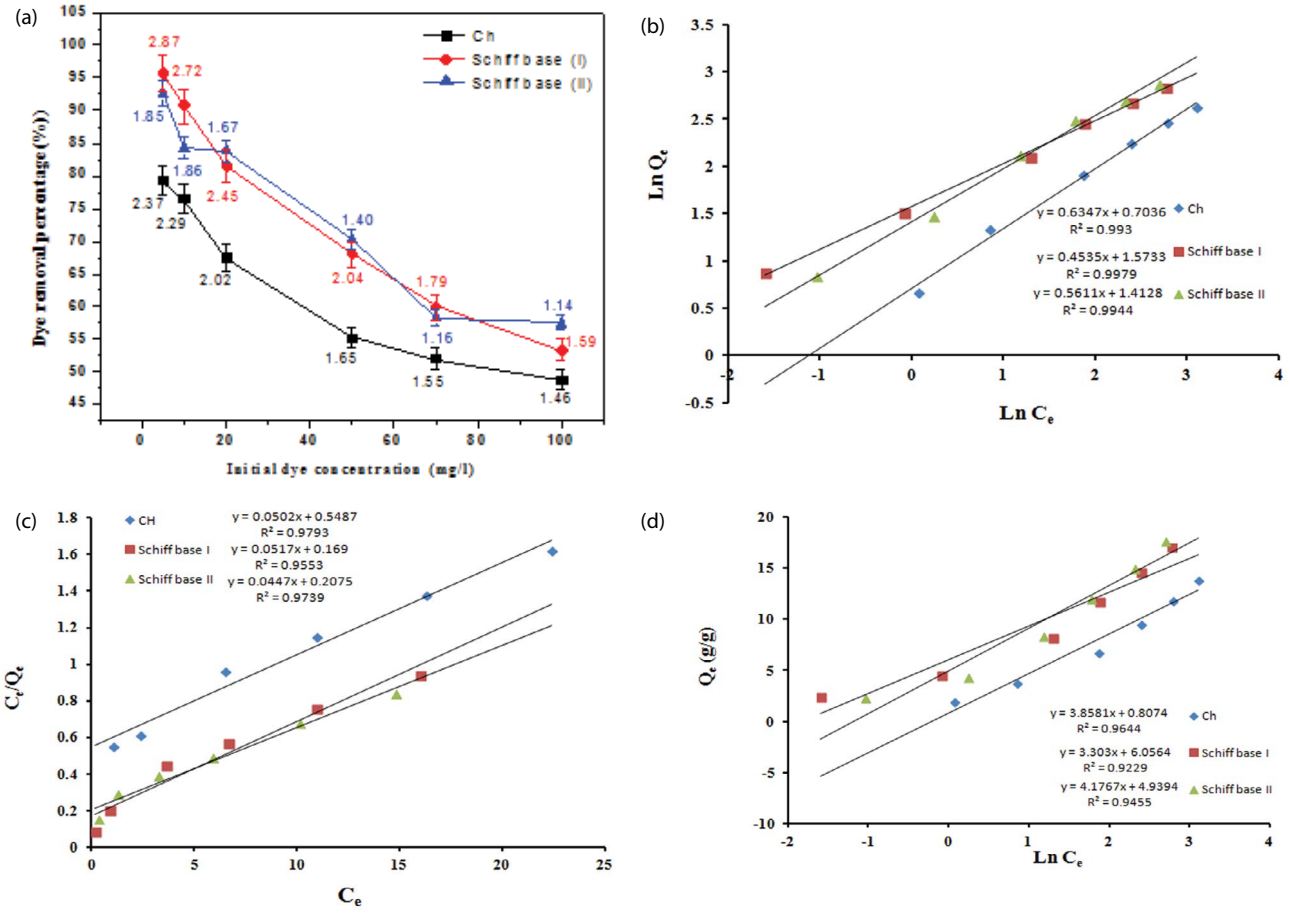

Fig. 12. (a) Effect of the initial dye concentration on their removing percent (%) using chitosan (Ch), chitosan Schiff base (I) and chitosan Schiff base (II) adsorbents (pH 4.0, 180 min, 25°C, 250 rpm, 0.05 g), (b) Freundlich isotherm, (c) Langmuir isotherm, and (d) Temkin isotherm.

bases (I) and (II), respectively, indicating mathematical fit adsorption date but less than the Freundlich model.

Langmuir parameters for the MO anions removal, q_m, and K were calculated from the slope and intercept of Fig. 12c and presented in Table 7. The maximum adsorption capacity for the chitosan, chitosan Schiff (I), and chitosan Schiff (II) was found 19.92, 19.34, and 22.37 mg/g, respectively.

To predict whether an adsorption system is favourable or unfavourable, (dimensionless separation factor), which consider essential characteristics of the Langmuir isotherms, is calculated. R_L defined as [70]:

$$R_L = \frac{1}{1 + KC_0} \tag{14}$$

Values of R_L (Table 8) for the MO anions removal falls between zero and one show favourable adsorption [71], which confirmed that the adsorption of the MO anions onto the chitosan, chitosan Schiff (I), and chitosan Schiff (II) under the conditions used in this study was favourable by Langmuir isotherm.

Temkin isotherm considered the effects of indirect adsorbent/adsorbate interactions on the adsorption process. The heat of adsorption of all the molecules in the layer would decrease linearly with coverage due to adsorbent/adsorbate interactions [72]. It can be expressed in the linear form as [73,74]:

$$q_e = B \ln K_T + B \ln C_e \tag{15}$$

A plot of q_e vs. $\ln C_e$ (Fig. 12d) enables the determination of the isotherm constants B_T and K_T from the slope and the intercept. From Fig. 12d, the calculated K_T equal to 1.233, 6.255, and 3.262 L/g for chitosan adsorbent and the chitosan Schiff bases (I) and (II), respectively, which represent the equilibrium binding constant corresponding to the maximum binding energy however, the constant B_T that equal to 3.858, 3.303, and 4.1767 J/mol for chitosan adsorbent and the chitosan Schiff bases (I) and (II), respectively, is related to the heat of adsorption (Table 9).

Table 6
Parameters of the Freundlich isotherm and correlation coefficients for the adsorption of MO dye

Adsorbent	η_f	K_F (g/g)	R^2
Ch	1.576	2.021	0.993
Schiff base (I)	2.205	4.822	0.9979
Schiff base (II)	1.782	4.107	0.9944

Table 7
Parameters of the Langmuir isotherm and correlation coefficients for the adsorption of MO dye

Parameter	Ch	Schiff base (I)	Schiff base (II)
Q_{max} (mg/g)	19.92	19.34	22.37
K (L/g)	10.93	11.97	4.64
R^2	0.9793	0.9553	0.9739

Table 8
R_L values of the Langmuir isotherm

MO, ppm	Ch	Schiff base (I)	Schiff base (II)
5	0.01797	0.01643	0.04132
10	0.00906	0.00828	0.02109
20	0.00455	0.00416	0.01066
30	0.00304	0.00278	0.00713
40	0.00228	0.00208	0.00535
50	0.00182	0.00167	0.00429

Table 9
Parameters of the Temkin isotherm and correlation coefficients for the adsorption of MO dye

Temkin parameters	Ch	Schiff base (I)	Schiff base (II)
B_T (J/mol)	3.858	3.303	4.1767
K_T (L/g)	1.233	6.255	3.262
R^2	0.9644	0.9229	0.9455

Considering the R^2 values for the three isotherm models, the Freundlich isotherm model gave the highest R^2 values, showing that the adsorption of the MO anions onto the chitosan adsorbent and the chitosan Schiff bases (I) and (II) adsorbents was best described by this model. This suggested that the formation of multi-layers of adsorption [75].

4. Conclusion

Novel crosslinked chitosan Schiff base derivates adsorbents were developed by the coupling of chitosan with 4-dimethylamino benzaldehyde, (chitosan Schiff base (I) and benzophenone, chitosan Schiff base (II)), for the adsorption of anionic reactive dye (Methyl orange) from aqueous solutions. The results showed a high-speed adsorption rate of the MO by the chitosan Schiff base derivates where removed 87%–94% after only 15 min while chitosan needs 180 min to remove the same MO %. Variation of the initial dye concentration reduced the removal percentage at a linear mode using fixed adsorbent dosage. Within the studied range of MO concentration, the developed chitosan Schiff bases adsorbents show a constant adsorption ability over wide ranges of temperature (25°C–80°C) and pH (4.0–9.0) of the MO contaminated wastewater. The pHzpc values of the chitosan (pHzpc value 7.6) and the chitosan Schiff base (I) and (II) adsorbents will following the order: chitosan > chitosan Schiff base (I) > chitosan Schiff base (II). That results in an additional contribution of the hydrophobic–hydrophobic interaction, which increased with pH from 38% to 94% of chitosan Schiff base (I) adsorbent and from 55% to 83% of chitosan Schiff base (II) adsorbent. The adsorption kinetics of MO dye was found to follow the pseudo-second-order model. The values of α estimated by Elovich kinetic model are 2.2786 and 2.0489 mg/g which close from the experimental values; 2.415 mg/g for chitosan Schiff base (I), and chitosan Schiff base (II). Following up the adsorption mechanism performed using intraparticle diffusion model.

The obtained results indicate the governed of the MO diffusion onto chitosan Schiff bases (I) and (II) by the boundary layer effect only. While that the removal process was governed by both surface removal and intraparticle diffusion in case of the chitosan adsorbent. At the same time, the Freundlich, Langmuir and Temkin isotherm models have been applied to the adsorption data and were found to follow the Freundlich isotherm. The Langmuir monolayer maximum adsorption capacities were found 19.92, 19.34, and 22.37 mg/g for the chitosan, chitosan Schiff base (I), and chitosan Schiff base (II), respectively. The thermodynamic nature of the adsorption process was extracted using Van't Hoff plot. The positive values for the ΔH indicate the endothermic nature of the adsorption process. The obtained behaviour nominates the developed chitosan Schiff bases hydrogels to work under a wide range of operational conditions.

References

[1] I.M. Banat, P. Nigam, D. Singh, R. Marchant, Microbial decolorization of textile-dyecontaining effluents: a review, Bioresour. Technol., 58 (1996) 217–227.

[2] T. Robinson, G. McMullan, R. Marchant, P. Nigam, Remediation of dyes in textile effluent: a critical review on current treatment technologies with a proposed alternative, Bioresour. Technol., 77 (2001) 247–255.

[3] M.-S. Chiou, H.-Y. Li, Equilibrium and kinetic modeling of adsorption of reactive dye on cross-linked chitosan beads, J. Hazard. Mater., 93 (2002) 233–248.

[4] X.Y. Yang, B. Al-Duri, Application of branched pore diffusion model in the adsorption of reactive dyes on activated carbon, Chem. Eng. J., 83 (2001) 15–23.

[5] M.S. Mottaleb, D. Littlejohn, Application of an HPLC-FTIR modified thermospray interface for analysis of dye samples, Anal. Sci., 17 (2001) 429–434.

[6] S.M. Burkinshaw, O. Kabambe, Attempts to reduce water and chemical usage in the removal of bifunctional reactive dyes from cotton: Part 2 bis(vinyl sulfone), aminochlorotriazine/vinyl sulfone and bis(aminochlorotriazine/vinyl sulfone) dyes, Dyes Pigm., 88 (2011) 220–229.

[7] P.C. Vandevivere, R. Bianchi, W. Verstraete, Treatment and reuse of wastewater from the textile wet-processing industry: review of emerging technologies, J. Chem. Technol. Biotechnol., 72 (1998) 289–302.

[8] C. O'Neill, F.R. Hawkes, D.L. Hawkes, N.D. Lourenço, H.M. Pinheiro, W. Delée, Colour in textile effluents – sources, measurement, discharge consents and simulation: a review, J. Chem. Technol. Biotechnol., 74 (1999) 1009–1018.

[9] A.J. Jafari, B. Kakavandi, R.R. Kalantary, H. Gharibi, A. Asadi, A. Azari, A.A. Babaei, A. Takdastan, Application of mesoporous magnetic carbon composite for reactive dyes removal: process optimization using response surface methodology, Korean J. Chem. Eng., 33 (2016) 2878–2890.

[10] Y. Ho, T. Chiang, Y. Hsueh, Removal of basic dye from aqueous solution using tree fern as a biosorbent, Process Biochem., 40 (2005) 119–124.

[11] G. Crini, Non-conventional low-cost adsorbents for dye removal: a review, Bioresour. Technol., 97 (2006) 1061–1085.

[12] L.D. Fiorentin, D.E.G. Trigueros, A.N. Módenes, F.R. Espinoza-Quiñones, N.C. Pereira, S.T.D. Barros, O.A.A. Santos, Biosorption of reactive blue 5G dye onto drying orange bagasse in batch system: kinetic and equilibrium modeling, Chem. Eng. J., 163 (2010) 68–77.

[13] C.P. Kaushik, R. Tuteja, N. Kaushik, J.K. Sharma, Minimization of organic chemical load in direct dyes effluent using low cost adsorbents, Chem. Eng. J., 155 (2009) 234–240.

[14] G.Z. Kyzas, A decolorization technique with spent "Greek Coffee" Grounds as zero-cost adsorbents for industrial textile wastewaters, Materials, 5 (2012) 2069–2087.

[15] G.Z. Kyzas, M. Kostoglou, A.A. Vassiliou, N.K. Lazaridis, Treatment of real effluents from dyeing reactor: experimental and modeling approach by adsorption onto chitosan, Chem. Eng. J., 168 (2011) 577–585.

[16] G.Z. Kyzas, N.K. Lazaridis, A.C. Mitropoulos, Removal of dyes from aqueous solutions with untreated coffee residues as potential low-cost adsorbents: equilibrium, reuse and thermodynamic approach, Chem. Eng. J., 189–190 (2012) 148–159.

[17] R.S. Juang, R.L. Tseng, F.C. Wu, S.H. Lee, Adsorption behavior of reactive dyes from aqueous solutions on chitosan, J. Chem. Technol. Biotechnol., 70 (1997) 391–399.

[18] D. Knorr, Dye binding properties of chitin and chitosan, J. Food Sci., 48 (1983) 36–37.

[19] G. Annadurai, L.Y. Ling, J.F. Lee, Adsorption of reactive dye from an aqueous solution by chitosan: isotherm, kinetic and thermodynamic analysis, J. Hazard. Mater., 152 (2008) 337–346.

[20] S. Chatterjee, S. Chatterjee, B.P. Chatterjee, A.K. Guha, Adsorptive removal of congo red, a carcinogenic textile dye by chitosan hydrobeads: binding mechanism, equilibrium and kinetics, Colloids Surf., A, 299 (2007) 146–152.

[21] F.A.A. Tirkistani, Thermal analysis of some chitosan Schiff bases, Polym. Degrad. Stab., 60 (1998) 67–70.

[22] J.E. dos Santos, E.R. Dockal, E′.T.G. Cavalheiro, Synthesis and characterization of Schiff bases from chitosan and salicylaldehyde derivatives, Carbohydr. Polym., 60 (2005) 277–282.

[23] A.M. Donia, A.A. Atia, K.Z. Elwakeel, Selective separation of mercury(II) using magnetic chitosan resin modified with Schiff's base derived from thiourea and glutaraldehyde, J. Hazard. Mater., 151 (2008) 372–379.

[24] H.M. Zalloum, Z. Al-Qodah, M.S. Mubarak, Copper adsorption on chitosan-derived Schiff bases, J. Macromol. Sci., Part A, 46 (2008) 46–57.

[25] E.A. Soliman, S.M. El-Kousy, H.M. Abd-Elbary, A.R. Abou-zeid, Low molecular weight chitosan-based Schiff bases: synthesis, characterization and antimicrobial activity, J. Food Technol., 8 (2013) 17–30.

[26] Y.N. Dai, P. Li, J.P. Zhang, A.Q. Wang, Q. Wei, Swelling characteristics and drug delivery properties of nifedipine-loaded pH sensitive alginate–chitosan hydrogel beads, J. Biomed. Mater. Res. Part B, 86B (2008) 493–500.

[27] S.P. Ramnani, S. Sabharwal, Adsorption behavior of Cr(VI) onto radiation crosslinked chitosan and its possible application for the treatment of waste water containing Cr(VI), React. Funct. Polym., 66 (2006) 902–909.

[28] M.S. Mohy Eldin, A.I. Hashem, A.M. Omer, T.M. Tamer, Preparation, characterization and antimicrobial evaluation of novel cinnamyl chitosan Schiff base, Int. J. Adv. Res., 3 (2015) 741–755.

[29] A. Pawlak, M. Mucha, Thermogravimetric and FTIR studies of chitosan blends, Thermochim. Acta, 396 (2003) 153–166.

[30] L.S. Guinesi, E.T.G. Cavalheiro, The use of DSC curves to determine the acetylation degree of chitin/chitosan samples, Thermochim. Acta, 444 (2006) 128–133.

[31] F.A.A. Tirkistani, Thermal analysis of some chitosan Schiff bases, Polym. Degrad. Stab., 60 (1998) 67–70.

[32] M.A. Hassan, A.M. Omer, E. Abbas, W.M.A. Baset, T.M. Tamer, Preparation, physicochemical characterization and antimicrobial activities of novel two phenolic chitosan Schiff base derivatives, Sci. Rep., 8 (2018) 11416, doi: 10.1038/s41598-018-29650-w.

[33] J. Estrela dos Santos, E.R. Dockal, É.T.G. Cavalheiro, Thermal behavior of Schiff bases from chitosan, J. Therm. Anal. Calorim., 79 (2005) 243–248.

[34] T.M. Tamer, M.A. Hassan, A.M. Omer, K. Valachová, M.S. Mohy Eldin, M.N. Collins, L. Šoltés, Antibacterial and antioxidative activity of O-amine functionalized chitosan, Carbohydr. Polym., 169 (2017) 441–450.

[35] E. Assaad, A. Azzouz, D. Nistor, A.V. Ursu, T. Sajin, D.N. Miron, F. Monette, P. Niquette, R. Hausler, Metal removal through synergic coagulation–flocculation using an optimized chitosan–montmorillonite system, Appl. Clay Sci., 37 (2007) 258–274.

[36] E.M. El-Sayed, T.M. Tamer, A.M. Omer, M.S. Mohy Eldin, Development of novel chitosan Schiff base derivatives for cationic dye removal: Methyl orange model, Desal. Water Treat., 57 (2016) 22632–22645.
[37] A. Szyguła, E. Guibal, M.A. Palacın, M. Ruiz, A.M. Sastre, Removal of an anionic dye (Acid Blue 92) by coagulation-flocculation using chitosan, J. Environ. Manage., 90 (2009) 2979–2986.
[38] B.H. Hameed, L.H. Chin, S. Rengaraj, Adsorption of 4-chlorophenol onto activated carbon prepared from rattan sawdust, Desalination, 225 (2008) 185–198.
[39] M.I. Temkin, V. Pyzhev, Kinetics of ammonia synthesis on promoted iron catalyst, Acta Physiochim. URSS, 12 (1940) 327–356.
[40] R.E. Khalifa, A.M. Omer, T.M. Tamer, W.M. Salem, M.S. Mohy Eldin, Removal of methylene blue dye from synthetic aqueous solutions using novel phosphonate cellulose acetate membranes: adsorption kinetic, equilibrium, and thermodynamic studies, Desal. Water Treat., 144 (2019) 272–285.
[41] H. Mahmoodian, O. Moradi, I. Tyagi, A. Maity, M. Asif, V.K. Gupta, Enhanced removal of Methyl orange from aqueous solutions by polyHEMA–chitosan-MWCNT nano-composite, J. Mol. Liq., 202 (2015) 189–198.
[42] L. Zhang, P. Hu, J. Wang, Q. Liu, R. Huang, Adsorption of Methyl orange (MO) by Zr(IV)-immobilized cross-linked chitosan/bentonite composite, Int. J. Biol. Macromol., 81 (2015) 818–827.
[43] T.K. Saha, N.C. Bhoumik, S. Karmaker, M.G. Ahmed, H. Ichikawa, Y. Fukumori, Adsorption of Methyl orange onto chitosan from aqueous solution, J. Water Resour. Prot., 2 (2010) 898–906.
[44] Y. Wang, G. Xia, C. Wu, J. Sun, R. Song, W. Huang, Porous chitosan doped with graphene oxide as highly effective adsorbent for Methyl orange and amido black 10B, Carbohydr. Polym., 115 (2015) 686–693.
[45] B. Tanhaei, A. Ayati, M. Lahtinen, M. Sillanpää, Preparation and characterization of a novel chitosan/Al_2O_3/magnetite nanoparticles composite adsorbent for kinetic, thermodynamic and isotherm studies of Methyl orange adsorption, Chem. Eng. J., 259 (2015) 1–10.
[46] M. Ozacar, I.A. Sengil, A kinetic study of metal complex dye sorption onto pinedust, Process Biochem., 40 (2005) 565–572.
[47] R.L. Tseng, Mesopore control of high surface area NaOH-activated carbon, J. Colloid Interface Sci., 303 (2006) 494–502.
[48] W.J. Weber, J.C. Morris, Kinetics of adsorption on carbon from solution, J. Sanit. Eng. Div. Am. Soc. Civ. Eng., 89 (1963) 31–59.
[49] K. Kannan, M.M. Sundaram, Kinetics and mechanism of removal of methylene blue by adsorption on various carbons—a comparative study, Dyes Pigm., 51 (2001) 25–40.
[50] M. Sarkar, P.K. Acharya, B. Bhaskar, Modeling the removal kinetics of some priority organic pollutants in water from diffusion and activation energy parameters, J. Colloid Interface Sci., 266 (2003) 28–32.
[51] G. Crini, H.N. Peindy, F. Gimbert, C. Robert, Removal of C.I. Basic Green 4 (Malachite Green) from aqueous solutions by adsorption using cyclodextrin-based adsorbent: kinetic and equilibrium studies, Sep. Purif. Technol., 53 (2007) 97–110.
[52] S.M. Venkat, D.M. Indra, C.S. Vimal, Use of bagasse fly ash as an adsorbent for the removal of brilliant green dye from aqueous solution, Dyes Pigm., 73 (2007) 269–278.
[53] T.A. Khan, S. Dahiya, I. Ali, Use of kaolinite as adsorbent: equilibrium, dynamics and thermodynamic studies on the adsorption of Rhodamine B from aqueous solution, Appl. Clay Sci., 69 (2012) 58–66.
[54] G. Zhao, J. Li, X. Wang, Kinetic and thermodynamic study of 1-naphthol adsorption from aqueous solution to sulfonated graphene nanosheets, Chem. Eng. J., 173 (2011) 185–190.
[55] M. Alkan, O. Demirbas, S.Ç.M. Dogan, Sorption of acid red 57 from aqueous solution onto sepiolite, J. Hazard. Mater., B116 (2004) 135–145.
[56] D.M. Ruthven, Principles of Adsorption and Adsorption Processes, John Wiley & Sons, New York, 1985, pp. 523–524.
[57] B. Noroozi, G.A. Sorial, H. Bahrami, M. Arami, Equilibrium and kinetic adsorption study of a cationic dye by a natural adsorbent—silkworm pupa, J. Hazard. Mater., 39 (2007) 167–174.
[58] I. Uzun, Kinetics of the adsorption of reactive dyes by chitosan, Dyes Pigm., 70 (2006) 76–83.
[59] W. Liu, S. Sun, Z. Cao, X. Zhang, K. Yao, W.W. Lu, An investigation on the physicochemical properties of chitosan/DNA polyelectrolyte complexes, Biomaterials, 26 (2005) 2705–11.
[60] G. Crini, P.M. Badot, Application of chitosan, a natural aminopolysaccharide, for dye removal from aqueous solutions by adsorption processed using batch studies: a review of recent literature, Prog. Polym. Sci., 33 (2008) 399–447.
[61] S.A. Chaudhry, M. Ahmed, S.I. Siddiqui, S. Ahmed, Fe(III)-Sn(IV) mixed binary oxide-coated sand preparation and its use for the removal of As(III) and As(V) from water: application of isotherm, kinetic and thermodynamics, J. Mol. Liq., 224 (2016) 431–441.
[62] T. Jóźwiak, U. Filipkowska, P. Szymczyk, M. Kuczajowska-Zadrożna, A. Mielcarek, M. Zyśk, The influence of chitosan deacetylation degree on Reactive Black 5 sorption efficiency from aqueous solutions, Progress on Chemistry and Application of Chitin and its Derivatives, 21 (2016) 83–92, doi: 10.15259/PCACD.21.08.
[63] H. Hou, R. Zhou, P. Wu, L. Wu, Removal of Congo red dye from aqueous solution with hydroxyapatite/chitosan composite, Chem. Eng. J., 211–212 (2012) 336–342.
[64] A. Szyguła, E. Guibal, M.A. Palacın, M. Ruiz, A.M. Sastre, Removal of an anionic dye (Acid Blue 92) by coagulation-flocculation using chitosan, J. Environ. Manage., 90 (2009) 2979–2986.
[65] M.S. Chiou, H.O. Pang-Yen, H.-Y. Li, Adsorption of anionic dyes in acid solutions using chemically crosslinked chitosan beads, Dyes Pigm., 60 (2004) 69–84.
[66] E.M. El-Sayed, T.M. Tamer, A.M. Omer, M.S. Mohy Eldin, Development of novel chitosan Schiff base derivatives for cationic dye removal: Methyl orange model, Desal. Water Treat., 57 (2016) 22632–22645.
[67] Y.S. Ho, Effect of pH on lead removal from water using tree fern as the sorbent, Bioresour. Technol., 96 (2005) 1292–1296.
[68] M.M. Dubinin, E.D. Zaverina, L.V. Radushkevich, Sorption and structure of active carbons I. Adsorption of organic vapors, Zhurnal Fizicheskoi Khimii, 21 (1947) 1351–1362.
[69] N. Unlü, M. Ersoz, Adsorption characteristics of heavy metal ions onto a low cost biopolymeric sorbent from aqueous solutions, J. Hazard. Mater., 136 (2006) 272–280.
[70] A. Mohammad, A.K.R. Rifaqat, A. Rais, A. Jameel, Adsorption studies on *Citrus reticulate* (fruit peel of orange): removal and recovery of Ni(II) from electroplating wastewater, J. Hazard Mater., 79 (2000) 117–131.
[71] A. Stolz, Basic and applied aspects in the microbial degradation of azo dyes, Appl. Microbiol. Biotechnol., 56 (2001) 69–80.
[72] B.H. Hameed, L.H. Chin, S. Rengaraj, Adsorption of 4-chlorophenol onto activated carbon prepared from rattan sawdust, Desalination, 225 (2008) 185–198.
[73] M.I. Temkin, V. Pyzhev, Kinetics of ammonia synthesis on promoted iron catalyst, Acta Physiochim. URSS, 12 (1940) 327–356.
[74] I.A.W. Tan, A.L. Ahmad, B.H. Hameed, Adsorption isotherms, kinetics, thermodynamics and desorption studies of 2,4,6-trichlorophenol on oil palm empty fruit bunch-based activated carbon, J. Hazard. Mater., 164 (2009) 473–482.
[75] N. Unlü, M. Ersoz, Adsorption characteristics of heavy metal ions onto a low cost biopolymeric sorbent from aqueous solutions, J. Hazard. Mater., 136 (2006) 272–280.